Swelling of a lava plug associated with a Vulcanian eruption at Sakurajima volcano, Japan, as revealed by infrasound record: Case study of the eruption on January 2, 2007

Akihiko Yokoo, Takeshi Tameguri and Masato Iguchi

Sakurajima Volcano Research Center, Disaster Prevention Research Institute, Kyoto University, 1722-19, Sakurajima Yokoyamacho, Kagoshima 891-1419, Japan.

Telephone: +81-99-293-2058

Fax: +81-99-293-4024

yokoo@svo.dpri.kyoto-u.ac.jp

Abstract

In order to clarify the time relation of the expansion of a gas pocket and failure of it's the overlying plug of lava during Vulcanian eruptions, infrasound records and video images of the Vulcanian eruption that occurred at Sakurajima volcano on January 2, 2007, were analyzed with respect to their origin times. Weak (≤3 Pa) and slowly increasing air pressure preceded the

impulsive compression phase by 0.25–0.32 s, and a longer-period rarefaction phase of infrasound waves was recognized at all microphone stations. The velocity of the compression phase was assumed to be supersonic (ca. 400 m/s) up to 850 m above the crater bottom from other recent explosions. On the other hand, the propagation velocity of the preceding weak signal was regarded to be similar to the air sound velocity because the lack of impulsiveness is unlikely to be related to the main compression phase. Therefore, the estimated origin time of the main compression phase was delayed by 0.5–0.7 s from the preceding phase. The origin time of the preceding phase coincided with the onset of the isotropic expansion process of the pressurized gas pocket, which was obtained by the waveform inversion of the explosion earthquake. In contrast, the origin time of the main impulsive phase coincided with the time when the expansion rate reached its peak. This observation suggests that the volumetric increase of the gas pocket caused swelling of the surface of the crater bottom and its subsequent failure. When the expansion velocity exceeded a threshold level, the main impulsive compression phase radiated with a high velocity by the sudden releases of the pressurized gases. The volumetric change at the source was estimated to be 280–560 m^3 from the preceding phase of the infrasound. This volume change indicates that the vertical displacement of the swelling ground was on the order of 1.0 m, assuming the radius of the lava plug was ca. 10 m.

Keywords: Sakurajima Volcano, Vulcanian Eruption, Infrasound Wave

Introduction

From the last decade, low-frequency microphones have been used world-wide for acoustic observation of volcanic eruptions. Network or array observations using these microphones have enabled the correct determination of vent locations of the source (Ripepe and Marchetti 2002; Johnson 2005), even if the eruptions are obscured by bad weather conditions or topography. This makes acoustic observations, in particular when coupled with seismometers and/or video cameras, a powerful tool to provide an integrated geophysical analysis for understanding eruption mechanisms and to infer the depth in the conduit. For eruptions at open-vent systems (Garcés and Hansen 1998; Ripepe et al. 2001; Gresta et al. 2004), mechanisms for infrasound generation, as determined from these observations, have been proposed as oscillations of a large elongated bubble at the air-magma interface (Vergniolle and Brandeis 1996; Vergniolle et al. 1996, 2004), bursting of pressurized bubbles (Rowe et al. 2000), and the explosive fragmentation of foaming magma (Ripepe et al. 2001).

Despite the common use of infrasound at open-vent explosive systems, their application on Vulcanian systems is still poor. With the aim of understanding the source mechanism of infrasound generation during Vulcanian activity, where a lava plug has been observed at the crater bottom (Stix et al. 1997; Ohminato et al. 2006) is destroyed by the explosion (Ishihara 1985), we can not tacitly assume the same mechanism inferred for Strombolian eruptions, in which an infrasound wave generated at the magma free surface that located at a depth of a few tens m within the vent and propagated from that source depth to the air, without interaction with choking materials (Ripepe et al. 2001, 2002). In other words, deformation of the materials would occur at the onset of the eruption.

Fig. 1

At Sakurajima volcano, located in southwestern Japan (Fig. 1), explosive Vulcanian eruptions have repeatedly occurred at the summit crater since 1955, and the number of events attained 7888 at the end of 2006. Infrasound waves have always accompanied these eruptions and they have been observed with the low-frequency microphones (Iguchi and Ishihara 1990) and evidenced the existence of a precursor phase followed by a major pressure phase (Sakai et al. 2001). Propagations of infrasound waves in the atmosphere above the crater have occasionally been recorded by video cameras as visualized shock waves (Ishihara 1985; Yokoo and Ishihara 2007). Although the propagation velocities and the peak over-pressures for the conspicuous compression phase of infrasound waves have been examined, the weak pressure increase ahead of the strong compression phase (Sakai et al. 2001) has not been taken into account in the considerations of the eruption mechanism.

The mechanisms and source dynamics of Vulcanian eruptions of Sakurajima have been mainly studied from a seismological perspective by many researchers (Iguchi 1994; Uhira and Takeo 1994), comparing the seismic signals with the acoustic phenomena (Ishihara 1985). From the analysis of explosion earthquakes and infrasound waves, Tameguri et al. (2002) summarized the sequence of explosive eruption processes as follows. A pressure wave originating from an isotropic expansion at a depth of 2 km propagated upward in a magma conduit with a speed of 1.4–1.9 km/s, and reached a highly-pressurized gas pocket, which was pre-existing at a depth of 300–500 m beneath the crater bottom, within 1 s.

The pressure wave then induced expansion of the gas pocket. Strong infrasound wave radiated within 0.3 s after the start of this expansion. Strain steps were also observed at the onset of these explosive eruptions using extensometers deployed in an underground tunnel. The strain steps were caused by an instantaneous pressure decrease that reflected the outburst of the preformed gas pocket (Ishihara 1990).

Thereby, as proposed from the perspective of macroscopic eruption dynamics by Kanamori et al. (1984), we could assume that the surface phenomena of Vulcanian eruptions are initiated by the “instantaneous failure” of the cap that seals a pressurized gas and magma at the top of the conduit. However, it is known that instant failure with zero in time would not be realistic (Iguchi et al. 2007). A finite time is required for the cap failure, and some kinds of signals associated with this process would be observable.

The Green’s function of the air, through which the infrasound waves pass from the source to the microphone, is much simpler than that for the propagation of seismic waves in the ground (Garcés 1997; Johnson 2005). Therefore, it is thought that infrasound records are good indicators for understanding eruption mechanisms, because they directly reflect the source information. In this report, we analyze the infrasound records and video images of the Vulcanian eruption that occurred at 17:53 on January 2, 2007 to determine the exact origin time of the infrasound wave. The time relation between the acoustic and seismic wave generations is then clarified with a higher time resolution at the source with an aim to confirm the process for destruction of the existent lava plug. The eruption analyzed in this investigation was the most vigorous within the last 4 years at Sakurajima volcano, although it was small scaled one compared with the 1970-1990s eruptions.

Observations

Low-Frequency Microphones and Seismometers

Fig. 1 shows the infrasound observation network at Sakurajima volcano with three low-frequency microphones (Aco, Type 3348/7144). This type of microphone has a flat frequency response in the range of 0.1–100 Hz. Sampling frequencies were 200 Hz at stations SVO and ARM, and 100 Hz at KUR. Eruption earthquakes were observed using three broadband seismometers (Akashi, JCP-1 with a flat response of 0.02–120 s, 200 Hz sampling) at stations HAR, ARI and KOM and one long-period seismometer (Akashi, JEP-6B3, 0.025–2.5 s, 200 Hz sampling) installed in a borehole at SBT (Fig. 1). All signals from these sensors were digitized at 24-bit resolution with time data calibrated by GPS and transmitted to SVO via telephone lines.

Video Monitoring Systems

Visual observations with accurate time calibrated by GPS were conducted simultaneously using two image monitoring systems installed at SVO and KUR, on both sides of Sakurajima volcano (Fig. 1). In the SVO system, the shutter timing of the digital camera module was controlled by the 1 PPS signal from a GPS clock module. Images taken by the camera were transmitted to a computer via IEEE1394 cable with a rate of 30 fps, and stored as jpeg formatted files. The other system installed at KUR used a high-sensitive analog TV camera (30 fps/NTSC). The time-code was directly inserted on the video images using a time-code generator synchronized with a 1 kHz oscillator, which was controlled by the 1 PPS signal from the GPS. These videos were recorded on a HD/DVD video deck. Video images captured by both systems were able to be compared with other records acquired with accurate timing system errors of $\leq \pm 1/60$ s.

Characteristics of Observed Data of the Vulcanian Eruption on January 2, 2007

Infrasound Waveforms

Fig. 2

Fig. 2 shows the observed infrasound waves associated with the explosive eruption on January 2, 2007. The infrasound waves were mainly composed of a first impulsive compression and subsequent longer-period rarefaction phases, similar to an N-shaped shock wave. After the two main phases, some oscillations indicating a return to the ambient pressure lasted approximately 10 s. The waveforms observed at different stations resembled each other. Cross correlation coefficients for the 5 s window from the onset were 0.72 (SVO-KUR), 0.73 (SVO-ARM) and 0.92 (KUR-ARM). Spectrograms computed by Fast Fourier Transfer in the 5.12 s time windows, and shifted 0.1 s steps, are also displayed with their waveforms in Fig. 2(a). The intensity of the waveforms was mainly concentrated in the frequencies lower than 3 Hz. The maximum amplitude of the first compression phase was 78 Pa at SVO.

Another important feature, that is small and gradually increasing pressure (≤ 3 Pa), was recognized 0.25–0.32 s before the onset of the main phase at all stations (Fig. 2(b)). This is referred to as the “preceding phase” after Sakai et al. (2001). The increasing rate of the air pressure in the preceding phase was not constant, but was slightly accelerated with time. This preceding phase was not due to the response of the microphones, but was a part of the infrasound wave itself. The same type of microphones as used here was successful for the capture of shock waves at field explosion experiments using dynamite. The captured shock waves started with an instantaneous pressure increase without a preceding phase (Kato et al. 1999).

Characteristics of the infrasound wave of the eruption examined in the present study were commonly found in the records of all 10 eruptions during the period from June 2006 to August 2007 at Sakurajima.

Video Images

Fig. 3

Images taken by the KUR system during the eruption are shown in Fig. 3. The passage of the strong compression phase of the infrasound wave is clearly visualized. Before the eruption, fumarolic steam drifted above the crater rim, as seen in the upper part of the images at 17:53:51-17:53:53. Some of this steam disappeared instantaneously in the image at 17:53:54, and then condensed steam appeared over the crater rim (the following images). After this sequence of phenomena, numerous incandescent ballistics and a dense volcanic cloud were ejected from the inside of the crater (the images after 17:53:57).

Analysis and Results

Source Location and Origin Time of the Preceding Phase of the Infrasound Wave

Source location (x_0, y_0) and origin time $t_{0\mathrm{prec}}$ of the preceding phase were estimated from the arrival times at the three microphone stations (Fig. 1). A grid search method was applied for determination of the location (x_0, y_0). Grid point

Fig. 4

(x, y) was set on the ground surface within the area of the summit crater (Fig. 4; 800×700 m, 10-m increment for each).

Firstly, the path length L_i from the source points (x, y) to the station i was calculated based on Minakami et al. (1970), using DEM (digital elevation model) data (surveyed on December, 2001). However, we modified the elevation data at the southeastern part of the summit crater (B-crater) as being filled with talus deposits until 700 m altitude, because it was found that on September 2004 the B-crater was buried and no significant topographical changes have been observed since then (Fig. 5). The method of Minakami et al. (1970) was not so special that it has been already accepted for researchers studying volcanic infrasound waves (e.g., Ruiz et al. 2007); namely, the path-length was assumed to be summative lengths of divided sub-paths above a topographic profile. The simplest one was a summation of two paths, those from the source to the crater margin and from the crater margin to the station.

Fig. 5

The tentative origin time t_{ten} at each point (x, y) was then calculated as

$$t_{\mathrm{ten}} = \frac{1}{N} \sum_i \left| t_{\mathrm{arr}i} - \frac{L_i}{c_{\mathrm{eff}i}(z)} \right|, \qquad (1)$$

where N is the number of microphone stations ($N = 3$) and $t_{\mathrm{arr}i}$ is the arrival times of the preceding phase at the station i. The preceding phase was regarded as propagating with an effective speed of sound $c_{\mathrm{eff}i}(z)$ at an altitude z along its path-line from the source to the station (Garcés et al. 1998). The reason for this was that the preceding phase had no impulsive nature (Fig. 2). $c_{\mathrm{eff}i}(z)$ is described as;

$$\begin{aligned} c_{\mathrm{eff}i}(z) &= c_{\mathrm{air}}(z) + w_i(z) \\ &= \sqrt{\gamma R T(z) / \overline{M}} + w_i(z) \end{aligned}, \qquad (2)$$

where $c_{\mathrm{air}}(z)$ is the speed of sound in the air, γ is the specific heat ratio (=1.4), R is the universal gas constant (8.3144 J K^{-1} mol^{-1}), $T(z)$ is the air temperature (K), $\overline{M}$ is the mean molar mass of the air (28.966×10^{-3} kg mol^{-1}) and $w_i(z)$ is the component of the wind velocity (m/s) along the infrasound path. $T(z)$ and $w_i(z)$ were calculated from the aerological weather data for every 100 m altitude. A grid search was conducted so as to minimize the standard deviation;

$$\Delta\varepsilon = \frac{1}{N} \sum_i \left| \left(t_{\mathrm{arr}i} - \frac{L_i}{c_{\mathrm{eff}i}(z)} \right) - t_{\mathrm{ten}} \right| . \qquad (3)$$

The minimum deviation provides the source location (x_0, y_0) and the corresponding t_{ten} is regarded as the origin time $t_{0\mathrm{prec}}$. The resultant source location (x_0, y_0) of the preceding phase of the infrasound wave is shown by a double circle with the contour lines of $\Delta\varepsilon$ in Fig. 4. The source of the wave was located in a lateral position from the center of the A-crater with a spatial resolution of NNE directed area of 85×40 m at $\Delta\varepsilon \le 0.05$ s. This deviation value was slightly larger than the error of reading of $t_{\mathrm{arr}i}$ (± 0.02 s). The corresponding origin time $t_{0\mathrm{prec}}$ was simultaneously estimated to be 17:53:51.97 with the minimum $\Delta\varepsilon = 0.007$ s. The potential error of $t_{0\mathrm{prec}}$ was in the range of ± 0.11 s within this considering area of $\Delta\varepsilon \le 0.05$ s.

Origin Time of the Impulsive Compression Phase of the Infrasound Wave

Next, the origin time $t_{0\mathrm{comp}}$ of the main impulsive compression phase of the infrasound wave was estimated from the video record. The passage of the impulsive compression phase was clearly observed in the video recorded by the KUR system (Fig. 3). It was recognized by the disappearance of floating fumarolic steam at the rim of the summit crater and the increase in luminance of the parts on the images. The increase in luminance was caused by the disappearance of dark-colored steam clouds on the bright sunset light background. Temporary changes of luminance at five regions in and around the steam clouds (small squares labeled a–e in Fig. 3) are shown in Fig. 6. A sudden increase in luminance at 17:53:53.50 $\pm$ 0.05 corresponds to the disappearance of the clouds, due to the arrival of the compression phase of the infrasound wave. Time errors in these videos were potentially only $\leq \pm$ 1/60 s; however, these phenomena were not sufficiently distinct in the space on the images to determine a rigid time of their appearance within that error range because the steam cloud had no fixed form with time. The resulting time data were, therefore, represented with an error of $\pm$ 0.05 s.

Fig. 6

The steam cloud which disappeared instantaneously with the passage of the main compression phase was positioned horizontally in an area of 20×50 m at the eastern crater rim at an altitude of 920–950 m (Figs. 3, 4 and 5). Hence, the path-length from the estimated source location (the double circle in Fig. 4) to the steam was estimated to be 410–432 m under the assumption of the same source location for both the preceding and main compression phases. As the disappearance of the cloud above the crater was not well traced during the eruption, the propagation velocity of the main impulsive compression phase was assumed to be approximately 400 m/s on average, with reference to the eruptions on April 19, 2006 and November 4, 2007 (392–411 m/s; see Appendix). As a result, the origin time $t_{0\mathrm{comp}}$ of the impulsive compression phase was determined to be 17:53:52.47–52.63 (Table 1). Even if we consider the variation of the propagation speed as 392–411 m/s, possible differences of $t_{0\mathrm{comp}}$ was estimated to be only ± 0.03 s.

Table 1

The origin time $t_{0\mathrm{comp}}$ of the impulsive compression phase was 0.5–0.7 s after the origin time $t_{0\mathrm{prec}}$ of the preceding phase (Fig. 7). Moreover, the time difference between the two phases at the source ($t_{0\mathrm{comp}} - t_{0\mathrm{prec}}$) was 0.2–0.4 s longer than the observed arrival time difference at the microphone stations (observed duration of the preceding phase; Δt_i =0.25–0.32 s). This discrepancy was caused by the differences in the propagation velocities from the source to the stations. Namely, the main phase of the infrasound wave ran after the preceding phase with a supersonic propagation speed (ca. 400 m/s) as an air shock wave. This speed

Fig. 7

obviously did not decrease until a distance of ca. 850 m away from the source (see Appendix).

Interpretation and Discussion

Origin Time of the Gas Pocket Expansion Revealed by Seismological Analysis

As already described by Ishihara (1985, 1990), the main phase of the infrasound wave radiated at the outbreak of a highly pressurized gas pocket beneath the crater bottom and propagated as an air shock wave. Tameguri et al. (2002) demonstrated that isotropic expansion at a depth of 300–500 m revealed by moment tensor analysis of explosion earthquakes is closely related with the occurrence time and amplitude of this shock wave. It was hypothesized that the preceding phase ahead of the main phase of the infrasound wave would be induced by an upward movement of the lava plug toward its failure, due to expansion of the gas pocket. To confirm this, the start time of expansion of the gas pocket was estimated by the waveform inversion of the explosion earthquake, based on the method of Tameguri et al. (2002). In the calculation, a triangle source time function was assumed for the moment velocity ($\dot{M}_0(t)$). In the observed waveforms associated

Fig. 8

with the eruption on January 2, 2007 (Fig. 8), the compressional P phase, the subsequent dilatation wave (D phase) and long-period larger motion (LP phase) were clearly recognized as usual explosion earthquakes (Tameguri et al., 2002).

Table 2

Fig. 9

The results of the calculation are summarized in Table 2 and Fig. 9. Moment tensor analysis of explosion earthquakes shows that an isotropic expansion generating the P phase occurred first at a depth of 0.9 km below the sea level at 17:53:51.23 (Fig. 9(a)). Cylindrical contraction then followed at the same depth (Fig. 9(b)), radiating a dilatational elastic wave (the D phase). Approximately 0.8 s after the beginning of the P-phase isotropic expansion, a shallower isotropic expansion occurred at 0.5 km above the sea level (Fig. 9(c); LP1 source), which corresponds to the excitation of the LP phase being closely related to the shock wave at 17:53:52.03. The squared residual for estimation of the origin time of this

Fig. 10

source is shown in Fig. 10, which indicates that the resultant origin time is accurate in the order of 0.1 s. The shallower expansion changed to a horizontal contraction 1.1 s later (Fig. 9(d); LP2 source).

A noteworthy point of this result is the time of the LP1 source generating the shallower expansion. The origin time of the shallower expansion ($t'_{0\mathrm{LP1}}$=52.03 s), evaluated from moment tensor analysis of the explosion earthquake, coincides with the origin time of the preceding phase of the infrasound wave ($t_{0\mathrm{prec}}$=51.97 s; Table 1) evaluated from the infrasound source searching. On the contrary the peak time of the moment velocity (t'_{peak}=52.58 s) is close to the origin time of the impulsive compression phase ($t_{0\mathrm{comp}}$=52.47–52.63 s) evaluated from video images. These two correspondences show not only that the main impulsive compression phase of the infrasound wave is certainly related to the shallower expansion source exciting the LP phase, but also that the radiation of the preceding phase is closely related to the expansion process. This seems to support our hypothesis that the preceding phase of the infrasound wave was firstly excited at the upward movement of the lava plug, which acted as a lid of the gas pocket. In addition, the coincidence of the origin time of the main impulsive phase with the peak time of the moment velocity of expansion suggests that the lava plug was destroyed at the time when the expansion velocity attained a peak, 0.5–0.7 s after the start of expansion.

Volumetric Change for Excitation of the Preceding Phase of the Infrasound Wave

In the locating procedure, the infrasound phase preceding the main shock wave has been assumed to be a pressure wave propagating at sound speed velocity (~340 m/s; Fig. 7), as a consequence of the non-implusive nature of the signal. Accordingly the air pressure change $p_i(t)$ observed at the various infrasound stations i during the preceding phase ($-\Delta t_i \leq t \leq 0$ in Fig. 2(b)) may be described as follows (Lighthill 1978; Vergniolle and Brandeis 1996);

$$p_i(t) = \frac{\rho_{\mathrm{air}}(z)}{2\pi L_i} \frac{d^2}{dt^2} V\left(t - L_i / c_{\mathrm{eff}i}(z)\right), \tag{4}$$

where $\rho_{\mathrm{air}}(z)$ and $V(t)$ are the air density (kg m^{-3}) and the volume of the source (m^3), respectively. $\rho_{\mathrm{air}}(z)$ is calculated from the aerological weather data (the atmospheric pressure $p_{\mathrm{air}}(z)$ (Pa), and $T(z)$) by the perfect gas law;

$$\rho_{\mathrm{air}}(z) = p_{\mathrm{air}}(z) \overline{M} / RT(z). \tag{5}$$

Hence, the source time function of the volume change could be inversely estimated from the observed pressure change of the preceding phase.

However, the whole waveform of the preceding phase could not be observed, because the preceding phase was covered with the subsequent main phase after the arrival of the main phase at the stations (dashed line in the source time function in Fig. 7). As the main impulsive compression phase was radiated 0.5–0.7 s after the origin time of the preceding phase, it is assumed that the preceding phase continued until the onset of the main phase, but it was overtaken and hidden by the main shock wave in the pressure records. Assuming that the volumetric change had the same increasing rate as that estimated from the moment velocity in the LP1 source (the period from the origin time to the peak time), it was expressed by a quadratic function of the time ($V \propto \int \dot{M}_0 dt = \alpha t^2$; Fig. 9 and Table 2). Therefore, we here extrapolated the volume change as if it was not hidden by the shock wave, by fitting the double-integration of the observed infrasound pressure data at the station ARM into these quadratic function (Fig. 11), which was the least distorted of the three stations data during the propagation because ARM has the shortest path-length from the source (ca. 2.8 km). Consequently, it was 280–560 m^3 considering with the variation of the time of $t_{0\mathrm{comp}} - t_{0\mathrm{prec}}$ as 0.5–0.7 s (Fig. 11). This estimated volumetric change at the source was equivalent to the

Fig. 11

height of the ground bulge, in the order of 1 m (0.9–1.8 m), assuming that the radius of the cylindrical lava plug was the observed value of ca. 10 m (Ishihara 1985). However, vertical displacement of considering lava plug were estimated to be 0.3–1.3 m from KUR and SVO data, which was slightly smaller values than those from ARM data, since volume changes were only 210–420 m^3 and 90–200 m^3, respectively. These discrepancies might suggest that some of our assumptions used here were insufficient or incorrect and this point in question would be open to further discussion. The source dynamics for generating preceding phase of infrasound wave associated with Vulcanian eruptions and their physical parameters are necessary to be made a much clearer from combining theoretical and observational approaches.

Time Sequence of Infrasound Wave Generation

The results presented and discussed here allow us to infer a complex source mechanism for the infrasound radiated by the Vulcanian eruption of Sakurajima volcano on January 2, 2007, as shown in Fig. 12. A deeper source (0.9 km bsl) is

Fig. 12

inferred to radiate a pressure wave within the conduit (stage 0), which once it reaches a shallower gas pocket (ca. 500 m asl), confined below a sealing lava plug, triggers its isotropic expansion (stage 1). This explosion leads to an upraise of the lava plug at the bottom of the crater and the upward process of the lava plug with a 0.5–0.7 s duration would radiate the preceding phase of the infrasound wave. The preceding phase was observed as a weak and gradual increase of the air pressure change at the microphone stations around the crater. The expansion rate of the gas pocket gradually accelerated and when it exceed a threshold level, the lava plug failed and a strong air shock wave, which propagated with a velocity of ca. 400 m/s, started to be radiated (stage 2). This was observed as the main phase of infrasound wave at the stations; a set of compression and rarefaction phases. After breakage of the lava plug (removal of the lid), the gas pocket still expanded isotropically, but its rate changed and began to decrease.

Conclusions

Infrasound of the recent Vulcanian eruption of Sakurajima volcano in 2007 was analyzed with video and seismic records. From the results of the analysis, several conclusions were obtained.

(1) In the infrasound waveforms associated with the eruption observed by low-frequency microphones, the preceding phase was clearly recognized. It was characterized by weak and slowly increasing air pressure and it preceded the onset of the main impulsive compression phase by 0.25–0.32 s.

(2) The origin time of the preceding phase, which was estimated from the arrival times at the stations, corresponds to the start time of the expansion for the pressurized gas pocket determined by waveform inversion of explosion earthquakes. On the other hand, the origin time of the main impulsive compression phase, which is estimated from video images, was close to the time when the expansion velocity of the gas pocket reached a peak value. The time difference between the origin times of the preceding and the main phases was 0.5–0.7 s at the source.

(3) The identification of different signals originating at sequential times point to a complex process generating infrasound from Vulcanian eruptions at Sakurajima volcano. At the eruption onset, a gas pocket sealed by a consolidated lava plug began to expand first, which induced swelling-up of the lava plug and this radiated the preceding phase of the infrasound wave. The expansion rate of the gas pocket gradually accelerated within 0.5–0.7 s and when it exceeded a threshold level, the swelling lava plug led to a failure. At this time, the main impulsive compression phase of the infrasound wave was radiated by the sudden release of pressurized gases. After the failure of the lava plug, the expansion rate changed and began to decrease.

Acknowledgements

The authors are grateful to all stuff members of SVO for their helpful support, especially to K. Ishihara for providing many constructive comments and fruitful suggestions. We also appreciate the Ministry of Land, Infrastructures and Transport Japan, Kokusai Kogyo, Co., Ltd. and Kagoshima Local Meteorological Observatory for providing data of the ARM microphone, the DEM data, and aerological weather data, respectively. Set-up, maintenance, and operation of the

KUR camera were supported by NHK (Japan Broadcast Association) and Y. Tashiro. Two reviewers, M. Ichihara and E. Marchetti, are thanked for constructive criticisms that much improved this manuscript. This work was financially supported by the 21st COE program for DPRI, Kyoto University (No. 14219301), Grant-in-Aid for Scientific Research (Nos. 14080203 and 18740277), and JSPS Research Fellowships for Young Scientists (No. 19·126).

Appendix A. Propagation Velocity of the Impulsive Compression Phase of an Infrasound Wave

The propagation velocities of a set of compression and rarefaction phases of the infrasound waves associated with the Sakurajima Vulcanian eruptions on 1980s were higher (440–570 m/s) than the speed of sound in air at a distance near to the source (Ishihara 1985; Yokoo and Ishihara 2007). Two recent cases of video images taken by the SVO monitoring systems were analyzed to estimate the travel speeds of these main phases, by the detection of sudden luminance changes along the propagation path of the wave.

At the eruption on April 19, 2006, a temporal condensation cloud caused by passage of the rarefaction phase of the infrasound wave appeared at 09:50:21.1.

Fig. A.1

This cloud formation was recognized as luminance increasing at altitudes ranging 1060–1265 m (Fig. A.1(a)). This range corresponds to the weather clouds existing before the eruption. By tracing the onset time of luminance changes in altitude at every 5 m, the apparent propagation velocity of the wave was estimated as 392 m/s (± 11 m/s) on average. A propagating wave was also observed as weak changes in brightness at altitudes of 1250–1600 m for the eruption on November 4, 2006 (Fig. A.1(b)). The onset time of the increase in brightness at altitudes of 1315–1660 m indicated that the velocity of the wave was 411 m/s (± 11 m/s). From these two results, the main phase of the infrasound waves were certainly faster (ca. 400 m/s) than the speed of sound in air at a distance near to the source (until 360–870 m above the crater bottom).

References

Garcés MA (1997) On the volcanic waveguide. J Geophys Res 102: 22,547–22,564

Garcés MA, Hansen RA (1998) Waveform analysis of seismoacoustic signals radiated during the Fall 1996 eruption of Pavlof volcano, Alaska. Geophys Res Lett 25: 1051–1054

Garcés MA, Hansen RA, Lindquist KG (1998) Traveltimes for infrasonic waves propagating in a stratified atmosphere. Geophys J Int 135: 255–263

Gresta S, Ripepe M, Marchetti E, D’Amico S, Coltelli M, Harris AJL, Privitera E (2004) Seismoacoustic measurements during the July-August 2001 eruption of Mt. Etna volcano, Italy. J Volcanol Geotherm Res 137: 219–230. DOI 10.1016/j.jvolgeores.2004.05.017

Iguchi M (1994) A vertical expansion source model for the mechanisms of earthquakes originated in the magma conduit of an andesitic volcano: Sakurajima, Japan. Bull Volcanol Soc Japan 54: 161–186

Iguchi M, Ishihara K (1990) Comparison of earthquakes and air-shocks accompanied with explosive eruptions at Sakurajima and Suwanosejima volcanoes (in Japanese with English Abstract). Ann Disas Prev Res Inst 33B: 1–12

Iguchi M, Yakiwara H, Tameguri T, Hendrasto M, Hirabayashi J (2007) Mechanism of explosive eruption revealed by geophysical observations at the Sakurajima, Suwanosejima and Semeru volcanoes. J Volcanol Geotherm Res. DOI10.1016/j.jvolgeores.2007.10.010

Ishihara K (1985) Dynamic analysis of volcanic explosion. J Geodyn 3: 327–349

Ishihara K (1990) Pressure sources and induced ground deformation associated with explosive eruptions at an andesitic volcano: Sakurajima volcano, Japan. In: Ryan M (ed) Magma transport and storage. John Willey and Sons, Chichester New York Brisbane Toronto Singapore, pp 335–356

Johnson JB (2005) Source location variability and volcanic vent mapping with a small-aperture infrasound array at Stromboli Volcano, Italy. Bull Volcanol 67: 1–14. DOI 10.1007/s00445-004-0356-8

Kanamori H, Given JW, Lay T (1984) Analysis of seismic body waves excited by the Mount St. Helens eruption of May 18, 1980. J Geophys Res 89: 1856–1866

Kato K, Oshima H, Sasatani T, Ichiyanagi M, Takahashi H, Goto A, Aoyama H (1999) 7. Report about geophysical measurements (in Japanese). In: Taniguchi H (ed) 98’ Research project on the measurement of volcanic explosions, pp 30–45

Lighthill J (1978) Waves in fluids. Cambridge Press, New York

Minakami T, Utibori S, Hiraga S, Miyazaki T, Gyoda N, Utunomiya T (1970) Seismometrical studies of volcano Asama, Part I. seismic and volcanic activities of Asama during 1934–1969. Bull Earthq Res Inst 48: 253–301

Ohminato T, Takeo M, Kumagai H, Yamashina T, Oikawa J, Koyama E, Tsuji H, Urabe T (2006) Vulcanian eruptions with dominant single force components observed during the Asama 2004 volcanic activity in Japan. Earth Planets Space 58: 583–593

Ripepe M, Marchetti E (2002) Array tracking of infrasonic sources at Stromboli volcano. Geophys Res Lett 29: L2076. DOI 10.1029/2002GL015452

Ripepe M, Ciliberto S, Scheava MD (2001) Time constrains for modeling source dynamics of volcanic explosions at Stromboli. J Geophys Res 106: 8713–8727

Ripepe M, Harris AJL, Carniel R (2002) Thermal, seismic and infrasonic evidences of variable degassing rates at Stromboli volcano. J Volcanol Geotherm Res 118: 285–297

Rowe CA, Aster RC, Kyle PR, Dibble RR, Schlue JW (2000) Seismic and acoustic observations at Mount Erebus Volcano, Ross Island, Antarctica, 1994–1998. J Volcanol Geotherm Res 101: 105–128

Ruiz MC, Lee JM, Johnson JB (2007) Source constraints of Tungurahua volcano explosion events, Bull Volcanol 68: 480–490

Sakai T, Churei M, Yoshida A (2001) Existence of preceding phase in waveforms of air-shocks accompanying explosive eruptions at Sakurajima volcano and Karymsky volcano (in Japanese). Abstr Volcanol Soc Japan, A16

Stix J, Torres RC, Narváez LM, Cortés GPJ, Raime JA, Gómez DM, Castonguay R (1997) A model of vulcanian eruptions at Galeras volcano, Colombia. J Volcanol Geotherm Res 77: 285–303

Tameguri T, Iguchi M, Ishihara K (2002) Mechanism of explosive eruption from moment tensor analysis of explosion earthquakes at Sakurajima volcano, Japan. Bull Volcanol Soc Japan 49: 197–215

Uhira K, Takeo M (1994) The source of explosive eruption of Sakurajima volcano, Japan. J Geophys Res 99: 17,759–17,789

Vergniolle S, Brandeis G (1996) Strombolian explosions. 1. A large bubble breaking at the surface of a lava column as a source of sound. J Geophys Res 101: 20,433–20,448

Vergniolle S, Brandeis G, Mareschal JC (1996) Strombolian explosions 2. Eruption dynamics determined from acoustic measurements. J Geophys Res 101: 20,449–20,466

Vergniolle S, Boichu M., Caplan-Auerbach J (2004) Acoustic measurements of the 1999 basaltic eruption of Shishaldin volcano, Alaska 1. Origin of Strombolian activity. J Volcanol Geotherm Res 137: 109–134. DOI 10.1016/j.jvolgeores.2004.05.003

Yokoo A, Ishihara K (2007) Analysis of pressure waves observed in Sakurajima eruption movies. Earth Planets Space 59: 177–181

Figure Captions

Fig. 1. Observation network of low-frequency microphones, seismometers and video cameras at Sakurajima volcano. Solid squares indicate the microphone stations (SVO, KUR and ARM). Three broadband seismometers were installed at ARI, HAR and KOM, and one long-period seismometer was installed at SBT (open circles). Video cameras were installed at SVO and KUR (open triangles).

Fig. 2. (a) Observed infrasound waveform with spectrogram for the eruption on January 2, 2007. Inset numbers are the maximum pressure amplitudes. (b) Close-up of the waveforms shifted by the arrival times of the main impulsive compression phase (shown by the arrows in (a)) to be zero in time.

Fig. 3. Selected images of the eruption taken by the KUR monitoring systems from 17:53:51 to 17:54:00. Disappearance of fumarolic steam caused by the passage of the impulsive compression phase of the infrasound wave is shown by the two circles in the image at 17:53:54. Luminance changes in five small squares shown in the image at 17:53:51 (a–e; 20×20 pix) were analyzed.

Fig. 4. Source location of the infrasound wave for the eruption on January 2, 2007 (double circle). The red contour lines represent the resultant $\Delta\varepsilon$. Source locations associated with the 10

eruptions during 2006–2007 are indicated by circles. The hatched area at the eastern crater rim indicates the location of the fumarolic steam that was visible from KUR (see Figs. 3 and 5).

Fig. 5. Aerial photograph of the summit crater of Sakurajima volcano (taken from the northeast on August 6, 2005; courtesy of SVO). The B-crater had been buried by talus deposits since September 2004. The white squared zone at the crater rim (lower left) denotes the fumarolic steam indicated by arrows in Fig. 3.

Fig. 6. Luminance changes in the five small squares shown in Fig. 3. Onset times of the impulsive compression phase of the infrasound wave are recognized as sudden increases in luminance (light-gray colored time; disappearance of fumarolic steam at the five regions).

Fig. 7. Schematic time-spatial relation for the generation and propagation of the infrasound wave.

Fig. 8. Vertical velocity waveform for the explosion earthquake on January 2, 2007, observed at HAR (Fig. 1) and the synthetic one (black solid and red broken lines, respectively). P, D and LP indicate the P-wave first, dilatational and largest long-period motions, respectively (Tameguri et al., 2002). Onsets of their phases were indicated by arrows.

Fig. 9. Resultant source time functions of moment rate for each phase of the explosion earthquake The periods (a) to (d) were the source times of the P , D, LP1 and LP2 phases, respectively. Details are in the text and Table 2.

Fig. 10. Reliability of the origin time of the LP1 source ($t'_{0\mathrm{LP1}}$) for the eruption on January 2, 2007. Residual is plotted against the time variation.

Fig. 11. Estimated volumetric change for an excitation of the preceding phase using pressure data observed at ARM (solid and dotted lines). Zero in time is set by the arrival time of the main phase at ARM. The dashed line at t>0 is assumed from the estimated moment change ($V \propto t^2$).

Fig. 12. Schematic sequential image for the surface phenomena at the explosive eruption of Sakurajima volcano on January 2, 2007. Stage 0: pressurized gas pocket is sealed with a consolidated lava plug. Stage 1: swelling up of the crater bottom, which excites a preceding phase of the infrasound wave, due to expansion of the gas pocket beneath the crater. Stage 2: the lava plug (crater bottom) is failed. At this time, the main phase of the infrasound wave is radiated. After the failure of the lava plug, the expansion rate of the gas pocket decreases.

Fig. A.1. (a) Snapshots before and during the eruption on April 19, 2006, taken by the SVO monitoring system (left), and luminance changes at several altitudes from 09:50:20 for this eruption (center: upward means brighten changing). Each arrow indicates the onset time of an increase in luminance. Relationship between these onset times and the altitude is displayed in the diagram with a 1.0 s window width (right). (b) Two captured images for the eruption on November 4, 2006, and luminance change during the 5 s above the crater of the eruption. After 17:33:40.8, weak increases in luminance were also observed.

Table 1. Estimated origin times for the infrasound wave and expansion of the shallower gas pocket.

		time (hh:mm:ss)
origin time of preceding phase	$t_{0\mathrm{prec}}$	17:53:51.97
origin time of main impulsive compression phase	$t_{0\mathrm{comp}}$	17:53:52.47–52.63
origin time of shallow gas pocket's expansion	$t'_{0\mathrm{LP1}}$	17:53:52.04
Peak time of expansion velocity of shallow gas pocket	t'_{peak}	17:53:52.58

Table 2. Results of the moment tensor analysis for the explosion earthquake on January 2, 2007.

	P phase	D phase	LP phase	
			LP1	LP2
source time of moment velocity (17:53:ss)				
origin time	51.23	51.43	52.03	53.13
peak time	51.33	51.73	52.58	53.73
end time	51.43	52.03	53.13	54.33
source depth (km bsl)	0.90	0.90	-0.50	-0.50
moment tensor (Nm)				

$\mathbf{M}_{xx}$	3.5×10^{11}	-16.1×10^{11}	5.8×10^{11}	-6.3×10^{11}
$\mathbf{M}_{yy}$	3.6×10^{11}	-17.2×10^{11}	6.1×10^{11}	-6.5×10^{11}
$\mathbf{M}_{zz}$	3.5×10^{11}	-8.1×10^{11}	6.0×10^{11}	-0.8×10^{11}
$\mathbf{M}_{xy}$	-0.2×10^{11}	0.6×10^{11}	-0.3×10^{11}	0.4×10^{11}
$\mathbf{M}_{xz}$	-0.1×10^{11}	0.9×10^{11}	-0.4×10^{11}	0.5×10^{11}
$\mathbf{M}_{yz}$	0.1×10^{11}	-0.5×10^{11}	0.2×10^{11}	-0.3×10^{11}

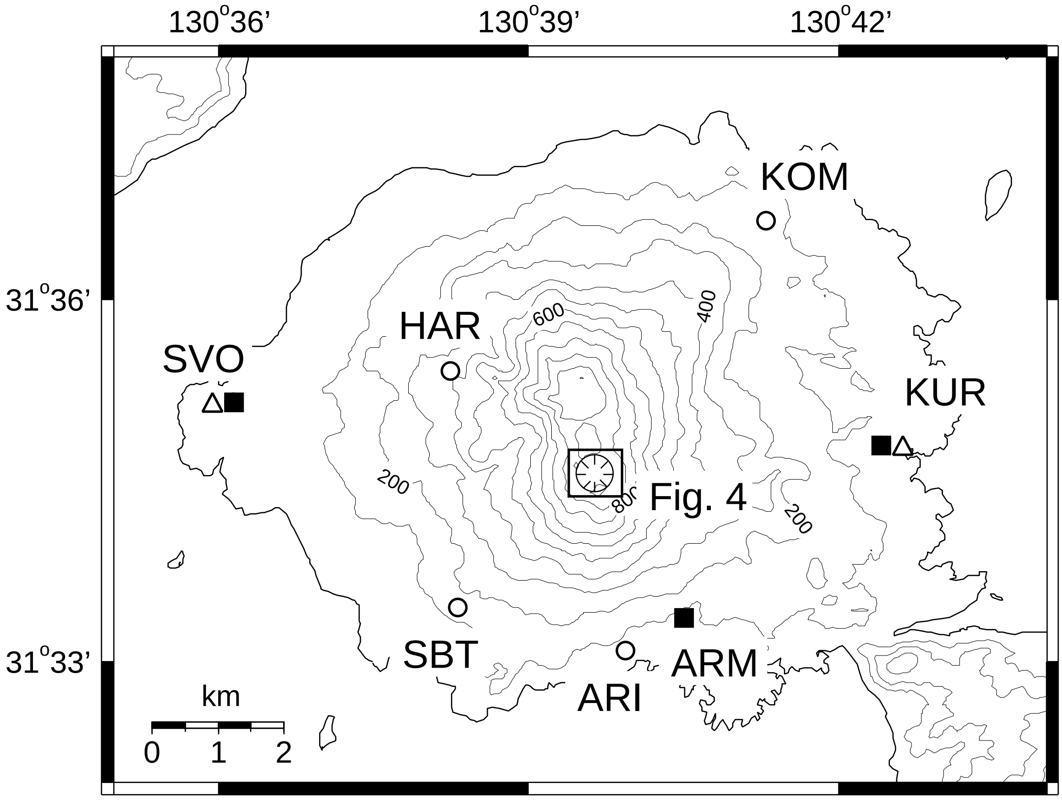

Figure 1: Yokoo et al.

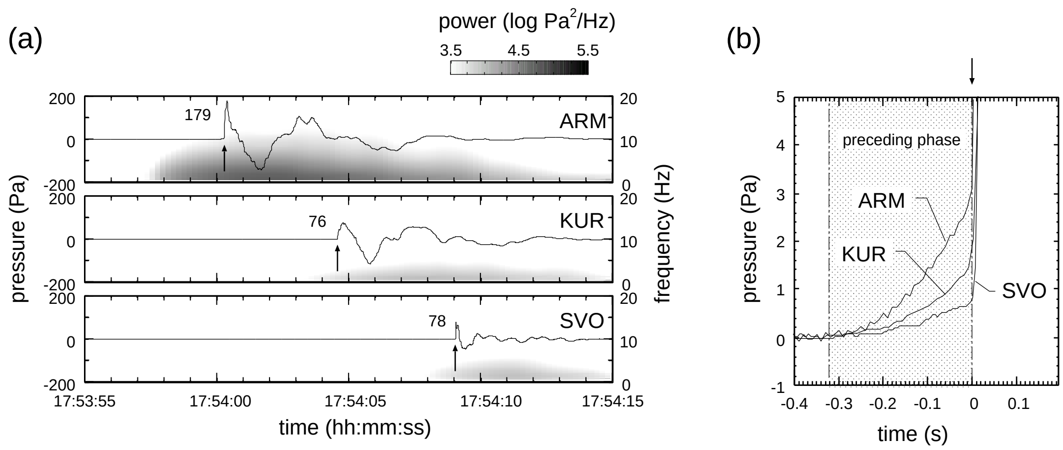

Figure 2: Yokoo et al.

Figure 3: Yokoo et al.

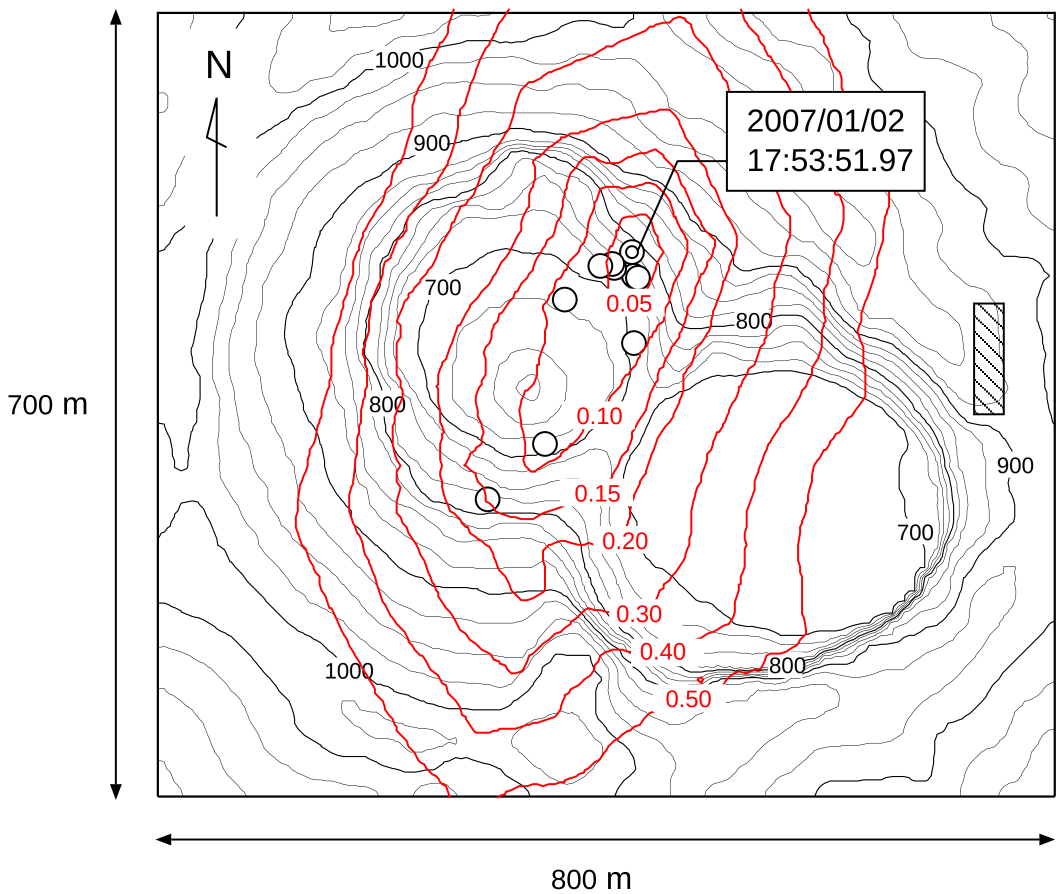

Figure 4: Yokoo et al.

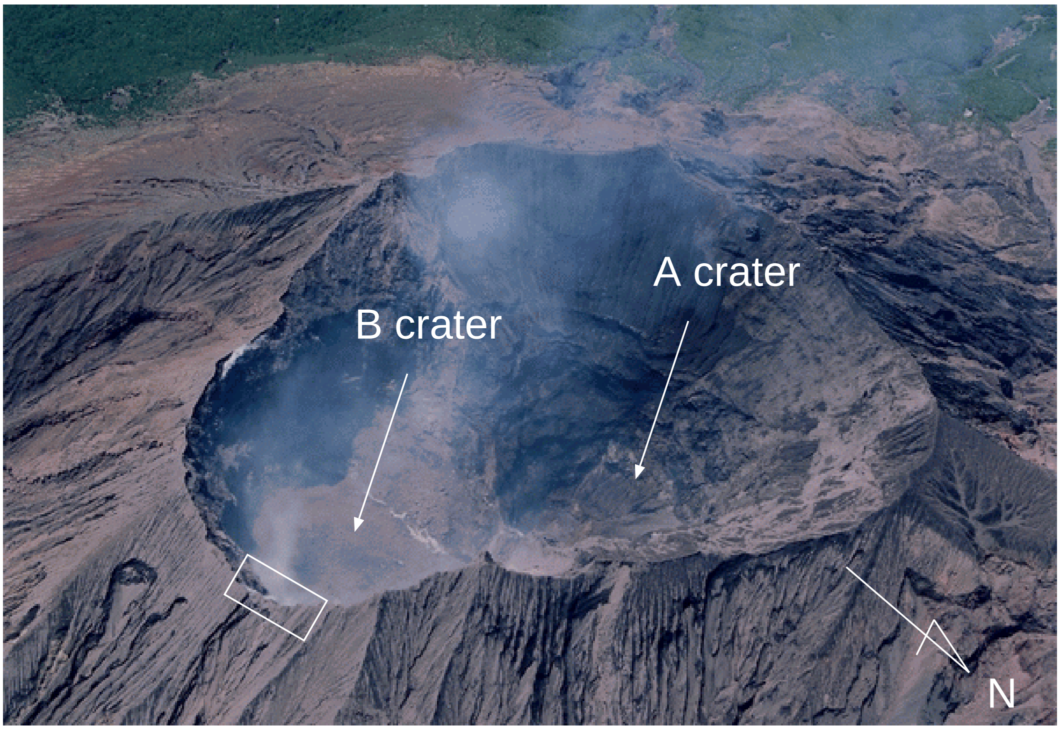

Figure 5: Yokoo et al.

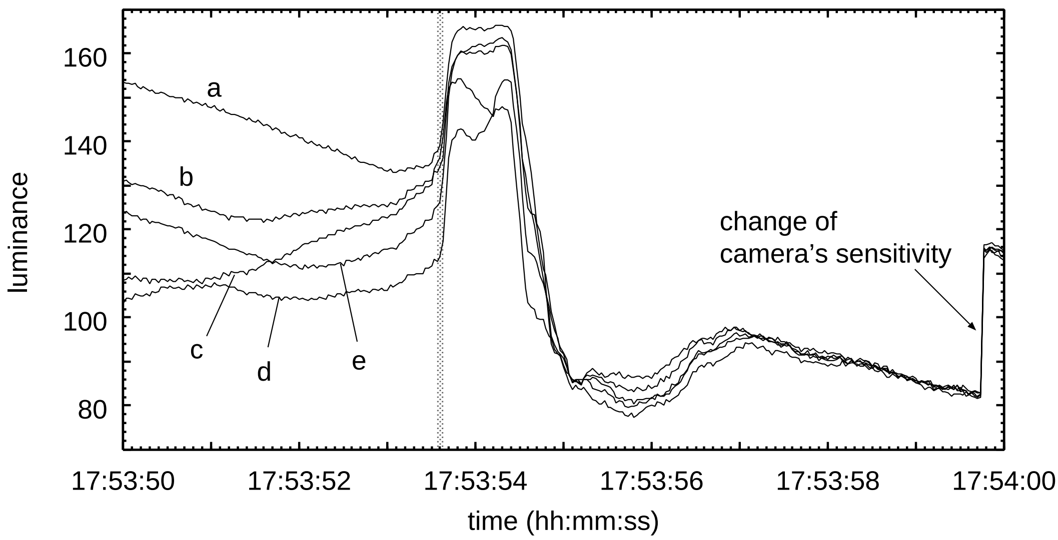

Figure 6: Yokoo et al.

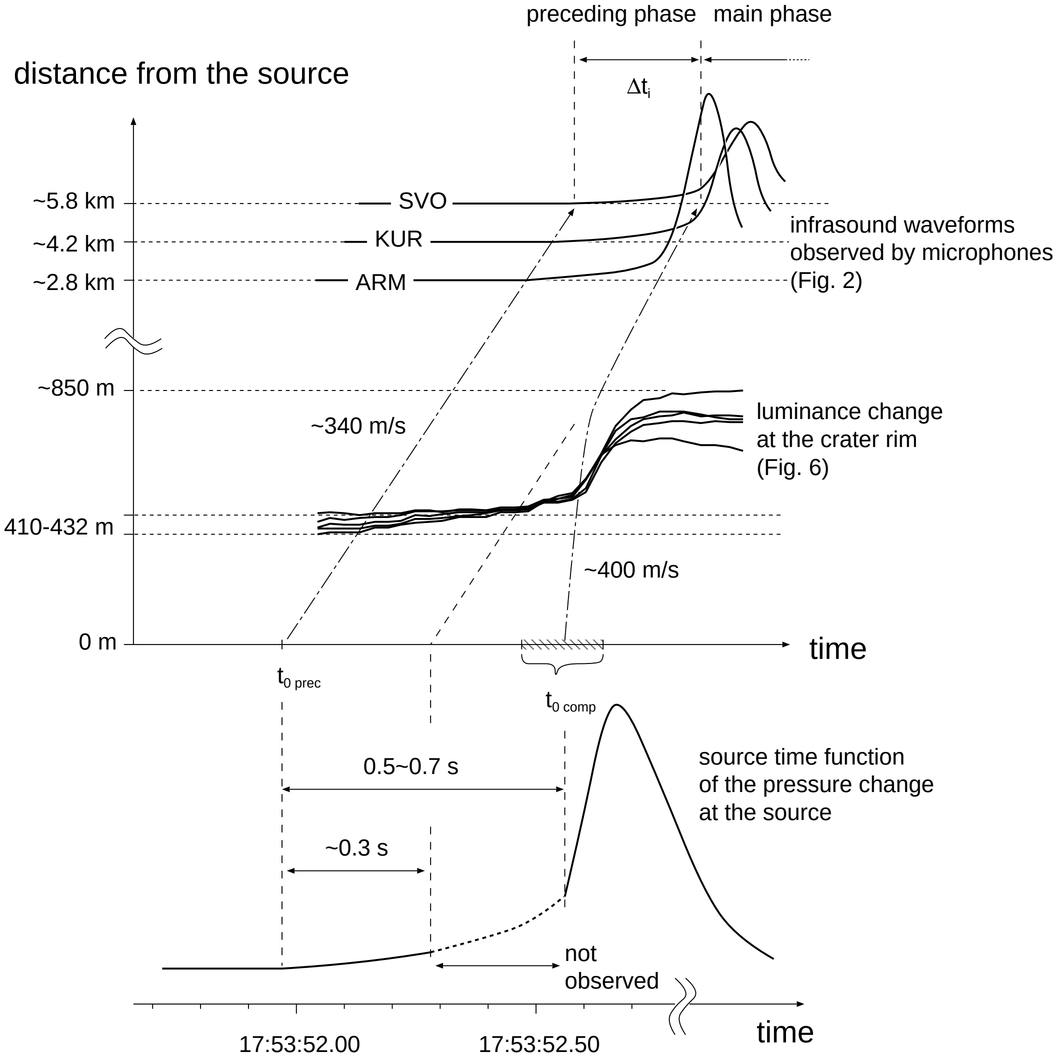

Figure 7: Yokoo et al.

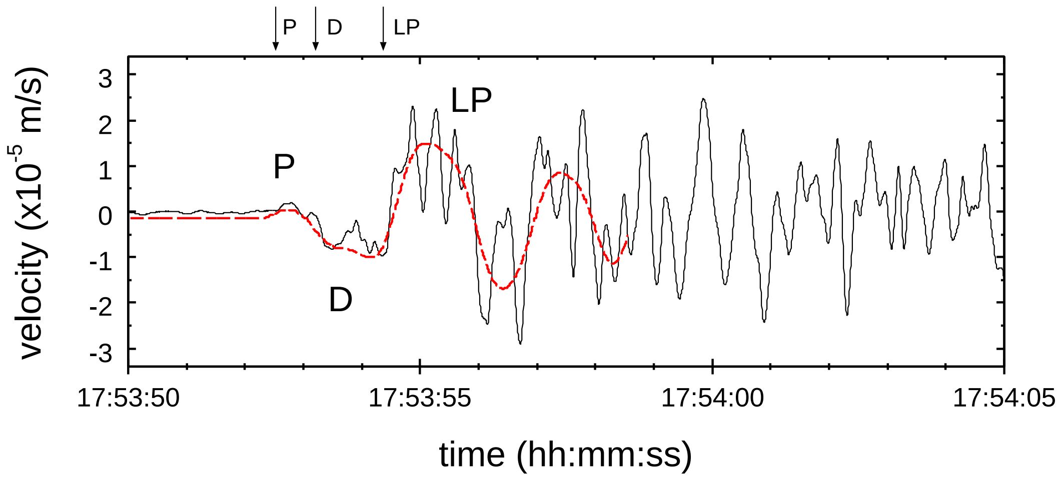

Figure 8: Yokoo et al.

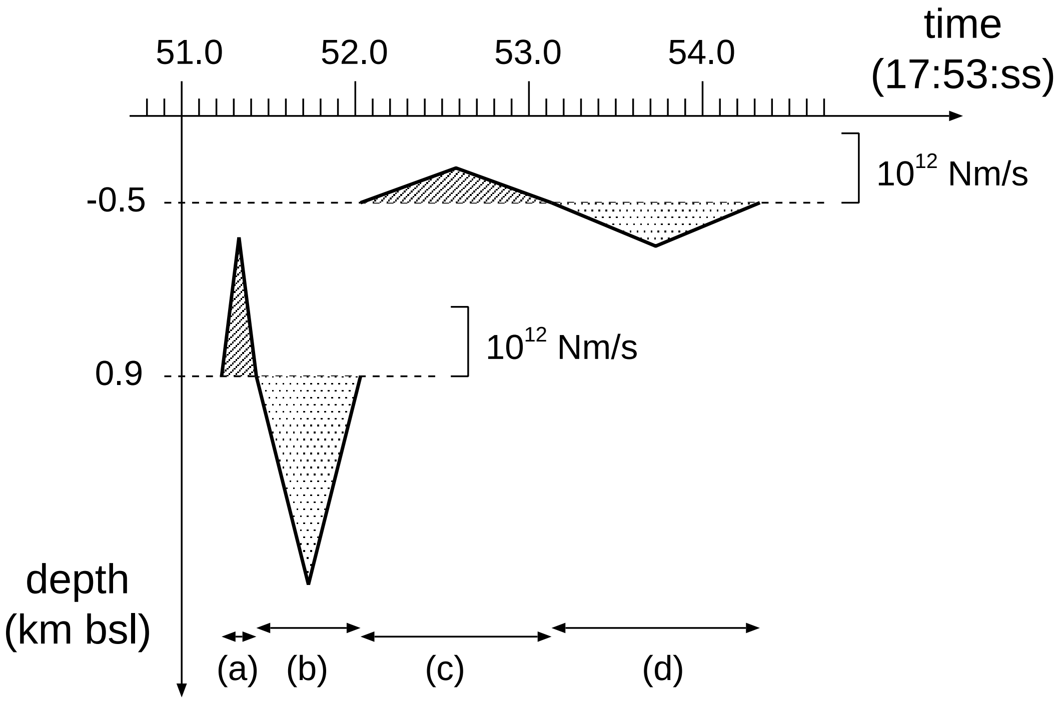

Figure 9: Yokoo et al.

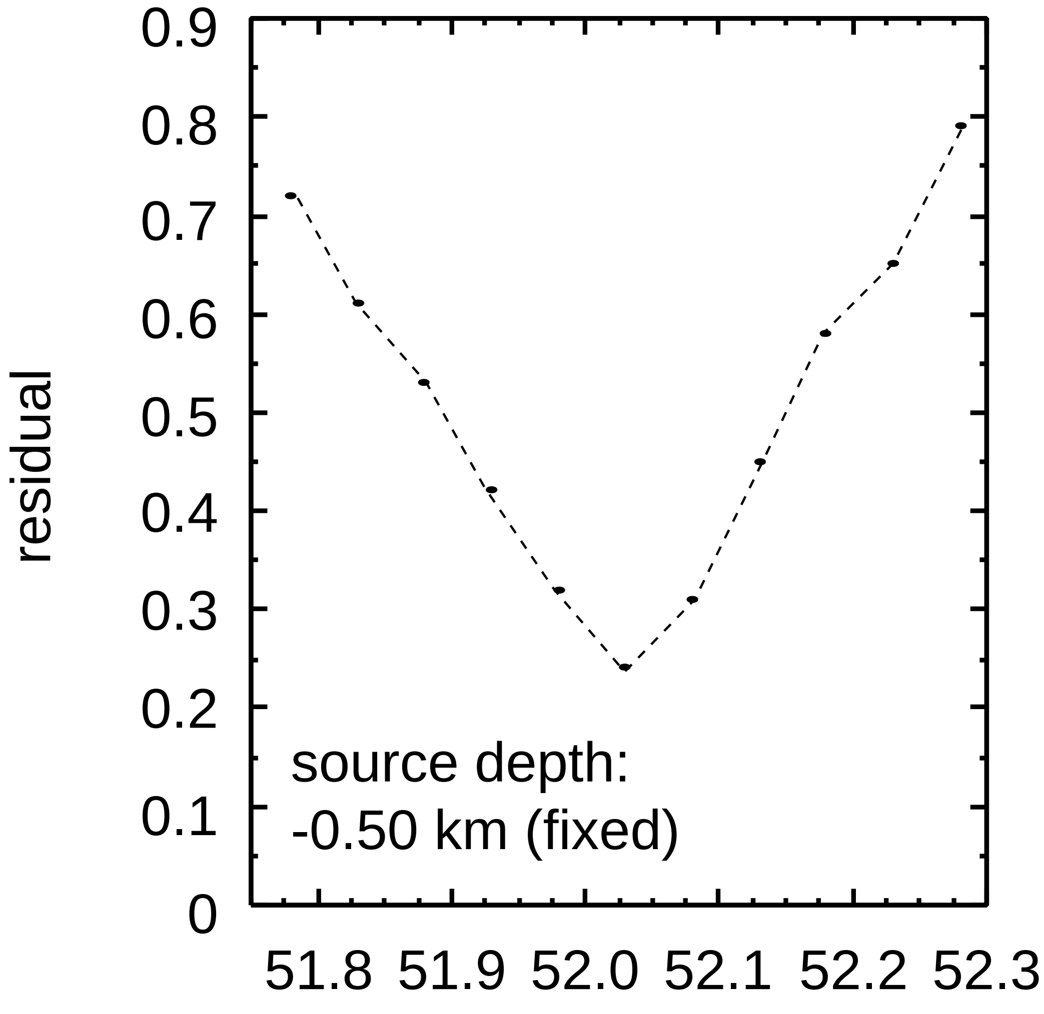

Figure 10: Yokoo et al.

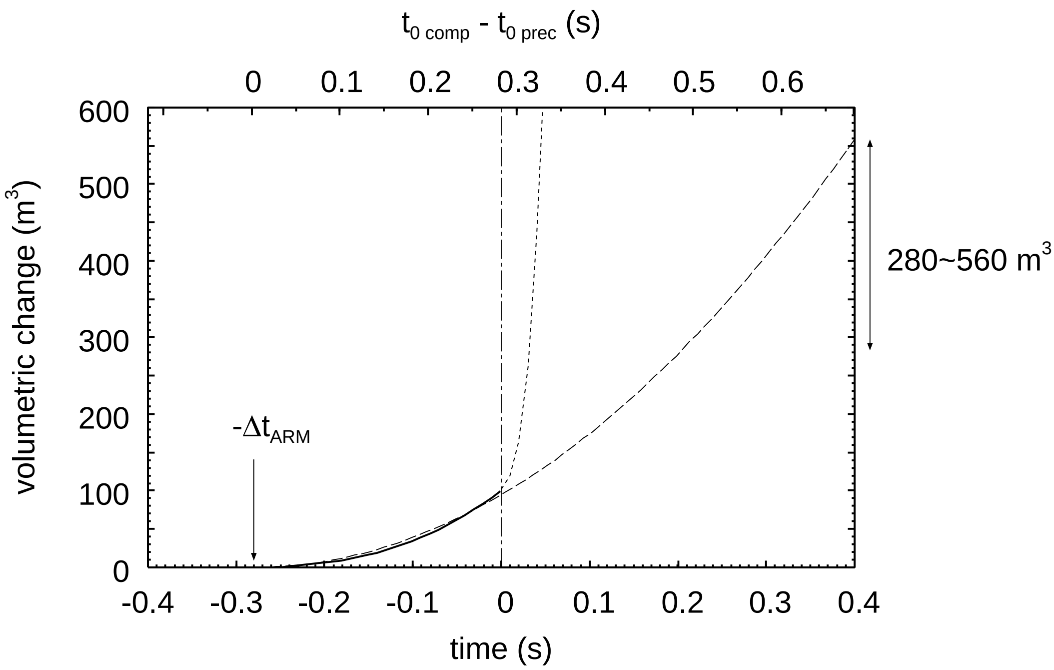

Figure 11: Yokoo et al.

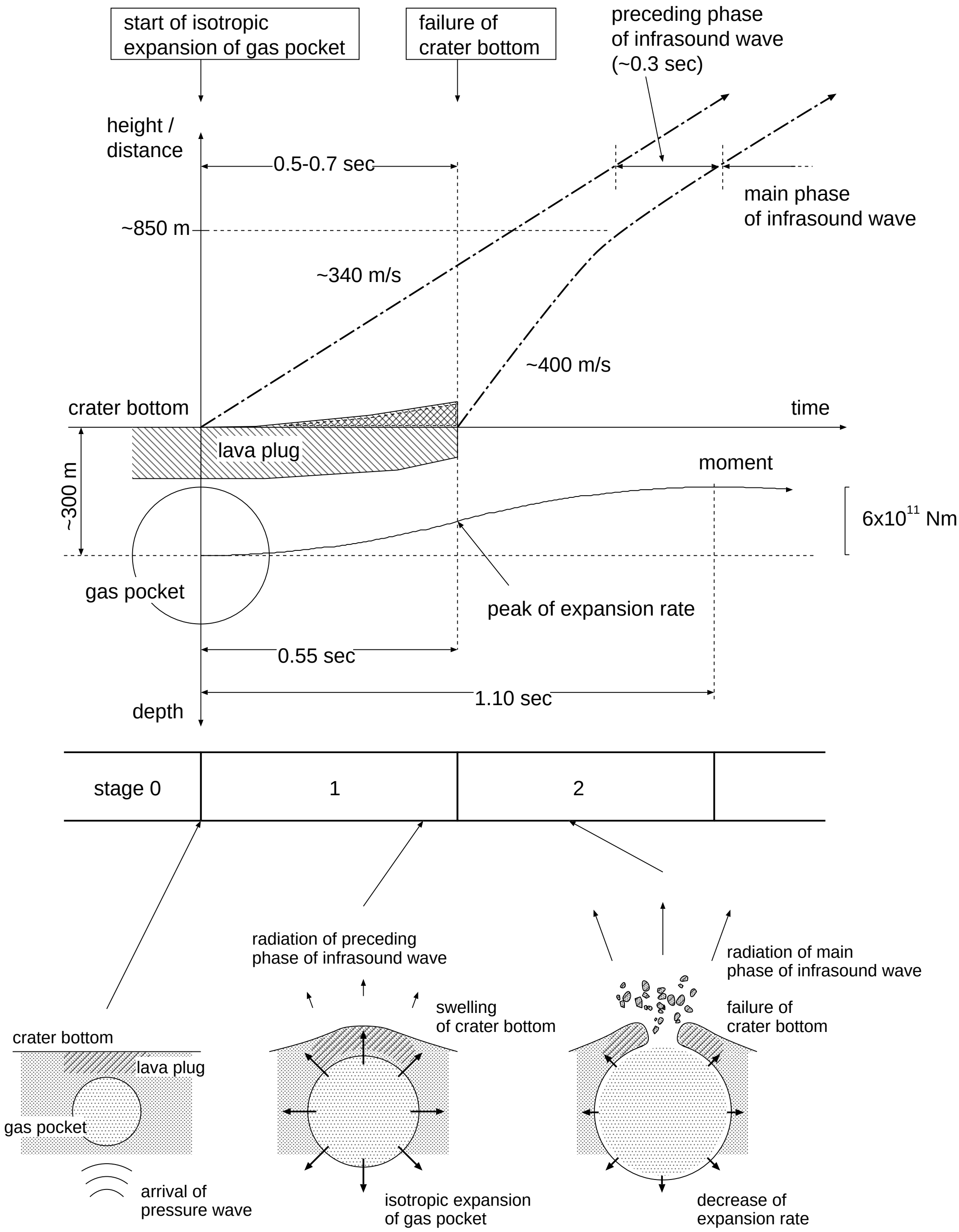

Figure 12: Yokoo et al.

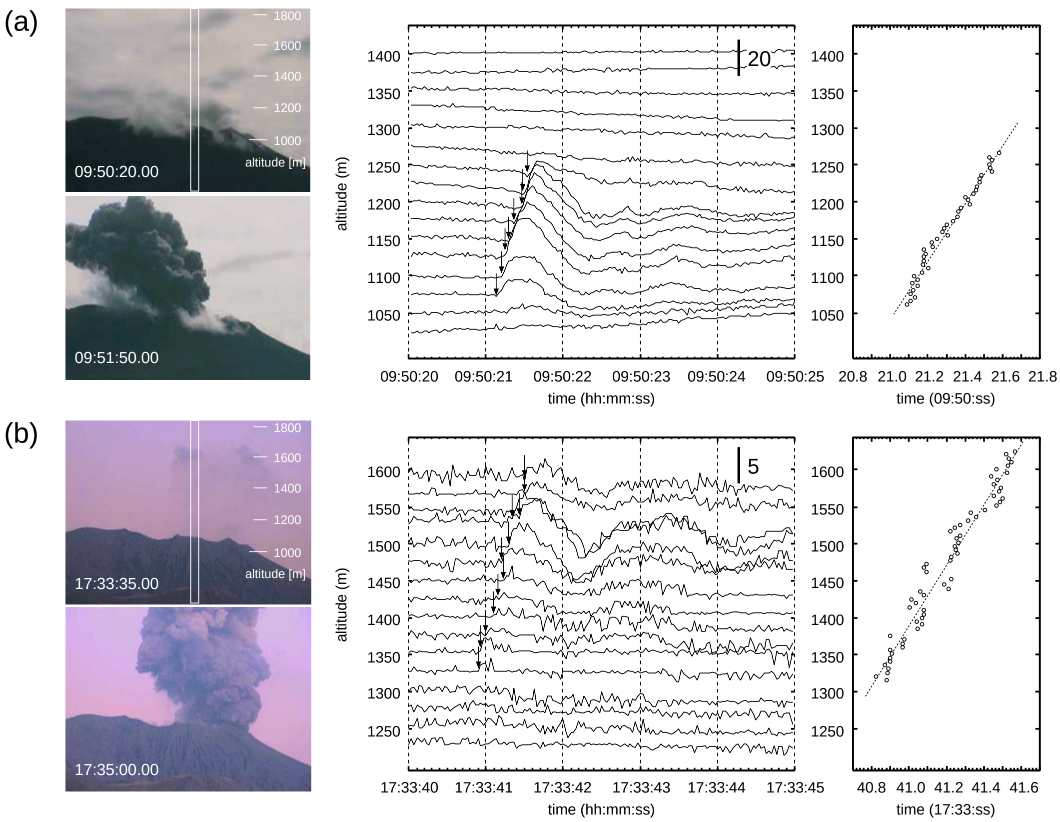

Figure 1: Yokoo et al.